# Preliminary Analysis on Reactivity Insertion Transient of Natural Circulation Reactor

Hyung Min Son [a*], Kune Yull Suh [b]
[a]*Korea Atomic Energy Research Institute, 989-111 Daedeok Daero, Yuseong Gu, Daejeon, 305-353, Korea*
[b]*Seoul National University, 1 Gwanak Ro, Gwanak Gu, Seoul 151-742, Korea*
[*]*Corresponding author: hyungmson@kaeri.re.kr*

## 1. Introduction

When a malfunction of the reactor control system occurs, there's a chance that the positive reactivity is inserted into the core, resulting in the increase of the core power. With the combination of the failure of the related safety features, this may raise the temperature of the core material beyond the design limit to break its integrity. For the fast nuclear reactors like FFTF and CRBRP, the overpower trip is initiated when the power reaches 115% of rated value to keep the fuel from melting [1]. In this study, the system response to the reactivity insertion transient on a liquid metal cooled natural circulation reactor is analyzed utilizing an in-house code based on a momentum integral model.

## 2. System Description and Analysis Results

This chapter first describes geometry of interest, neutronics data and then the transient simulation results are discussed.

### *2.1 Analysis Geometry and Assumptions*

Table 1 below summarizes a geometry and steady state operating condition of a typical 10 MWe natural circulation primary system cooled by liquid lead. Power conversion is performed by highly efficient Brayton cycle where its working fluid is supercritical carbon dioxide.

Table I: Primary System Description

| Parameters | Value |
|---|---|
| Thermal Power [MW] | 23.5 |
| Core Diameter [m] | 0.963 |
| Active Core Height [m] | 0.889 |
| Upper Gas Plenum Height [m] | 1.779 |
| Pitch-to-diameter Ratio | 1.189 |
| Number of Fuel Rods | 4,219 |
| Fuel Pin Diameter [cm] | 1.177 |
| Cladding Thickness [mm] | 0.401 |
| Number of Heat Exchanger Unit | 6 |
| Number of Tubes/Unit | 386 |
| Heat Exchanger Tube length [m] | 1.993 |
| Heat Exchanger Tube Outer/Inner Diameter [mm] | 15.112/11.717 |
| Heat Exchanger Pitch-to-diameter Ratio | 1.402 |
| Downcomer Outer/Inner Diameter [m] | 1.852/1.067 |
| Primary Mass Flow Rate [kg/s] | 1095.325 |
| Secondary Mass Flow Rate [kg/s] | 123.42 |
| Core Inlet/Outlet Temperature [K] | 706.17/853.13 |
| Heat Exchanger Inlet/Outlet Temperature [K] | 658.38/814.69 |

The power generation of the core is the results of the fission process inside the fuel materials and is proportional to the neutron generation rate. The behavior of the neutron density over time can be approximately described by following equation [2]:

$$\frac{P}{P_0} \cong \frac{\beta_{eff}}{\beta_{eff}-\rho} exp\left(\frac{\lambda\rho t}{\beta_{eff}-\rho}\right) - \frac{\rho}{\beta_{eff}-\rho} exp\left(-\frac{\beta_{eff}-\rho}{l^*}t\right) \quad (1)$$

where, $P$ is power (in W), the subscript 0 stands for initial steady-state value, $\beta_{eff}$ is effective delayed neutron fraction, $\rho$ is reactivity, $\lambda$ is weighted decay constant (in $s^{-1}$), t is time (in s), and $l^*$ is prompt neutron lifetime (in s).

The above kinetic parameters are estimated using McCARD code over the homogenized cylindrical core geometry [3]. Table 2 shows the evaluated parameter values along with reactivity coefficient averaged over temperature range from 600K to 1200K calculated using the same code. These data will be utilized in obtaining temperature and reactivity feedback effect on the power generation.

Table II: Summary of Kinetic Parameters

| Parameters | Value |
|---|---|
| Effective Delayed Neutron Fraction | 0.0039 |
| Weighted Decay Constant [$s^{-1}$] | 0.0984 |
| Prompt Neutron Lifetime [s] | 1.7009E-7 |
| Reactivity Coefficient, Fuel Pellet [$/K] | -3.6367E-4 |
| Reactivity Coefficient, Gap Bonding [$/K] | -4.5397E-4 |
| Reactivity Coefficient, Cladding [$/K] | -6.6776E-5 |
| Reactivity Coefficient, Coolant [$/K] | -2.2144E-3 |

In order to further simplify the calculation procedure, the secondary side boundary condition of the heat exchanger is held constant, and the effect of the thermal expansion of the core and structure on the flow cross section is neglected.

### *2.2 Transient Simulation Results*

In order to calculate the thermal-hydraulic behavior of the primary coolant, following momentum and energy equations are descritized and solved numerically over time using Newton-Raphson method and FEM

(Finite Element Method), respectively [4,5,6]. In addition, an extra energy equation is solved for each fuel pin material region to evaluate the structural temperature distribution [7].

$$\int_0^L \frac{\partial G}{\partial t} dz + \frac{G^2}{\rho}\Big|_{z=L} - \frac{G^2}{\rho}\Big|_{z=0} = P_{z=0} - P_{z=L} - \int_0^L \frac{f|G|G}{2D_e\rho} dz - \int_0^L \rho g dz \quad (2)$$

$$\rho c_p \frac{dT}{dt} = k\frac{d^2T}{dz^2} + \dot{q}'''_{gen} - \frac{\dot{m}c_p}{A_c}\frac{dT}{dz} \quad (3)$$

where, $L$ is total flow length (in m), $G$ is mass flux (in kg/m$^2$-s), $z$ is axial flow distance (in m), $\rho$ is coolant density (in kg/m$^3$), $P$ is pressure (in Pa), $f$ is friction factor, $D_e$ is equivalent hydraulic diameter (in m), $g$ is constant of gravitation (in m/s$^2$), $c_p$ is specific heat at constant pressure (J/kg-K), $T$ is temperature (in K), $k$ is thermal conductivity (W/m-K), $\dot{q}'''_{gen}$ is volumetric heat generation rate (W/m$^3$), and $A_c$ is the cross sectional flow area (m$^2$).

In first simulation, it is assumed that the reactivity is added to the core at the constant rate (ramp reactivity insertion) and the reactivity feedback is not considered. The range of the ramp spans from 1 to 10 cents/sec, where from CRBRP the maximum value from control rod malfunction is reported to be less than 3 cents/sec [8]. Figure 1 shows the change in the normalized power with respect to normal operating condition. We can see that even for the small reactivity insertions, the core power exceeds the design limit (115%) within 10 seconds. These points of intersection correspond to the time when the reactor shutdown system (insertion of shutdown rod) starts to act. Figures 2 and 3 show the change of the maximum temperature of the fuel centerline and the cladding from central pin over time following the reactivity insertion. Here, the constant steady state coolant mass flow rate is assumed. The calculation shows that for the higher ramp reactivity insertions (10 cents/sec), the high porosity formation is initiated in the pellet center less than 10 seconds, and even begins to melt around 6 seconds. From the cladding temperature data, it is seen that the two constraints pose more severe restrictions to the operation of the plant. Throughout this chapter, following relative temperature values are used for comparison purpose, where the initial values are taken from the steady state condition [8].

$$T_{FPc}^{relative}(t) = \frac{T_{FPc}(t) - T_{CLinlet}(0)}{T_{FPc}(0) - T_{CLinlet}(0)} \quad (4)$$

$$T_{CD}^{relative}(t) = \frac{T_{CD}(t) - T_{CLinlet}(0)}{T_{CD}(0) - T_{CLinlet}(0)} \quad (5)$$

where, subscripts FPc, CD, and CLinlet correspond to fuel centerline, cladding bulk, and coolant inlet, respectively.

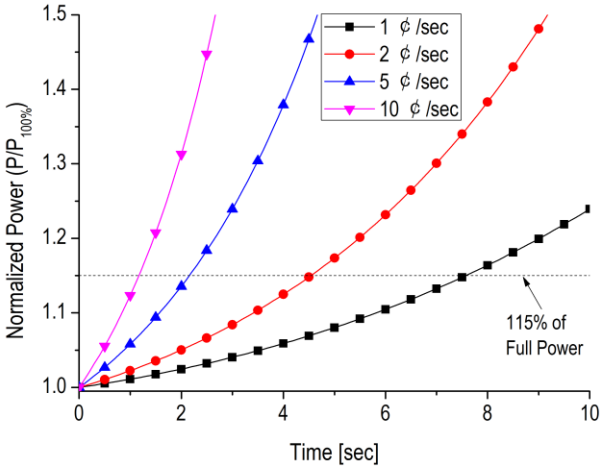


Fig. 1. Evolution of core power.

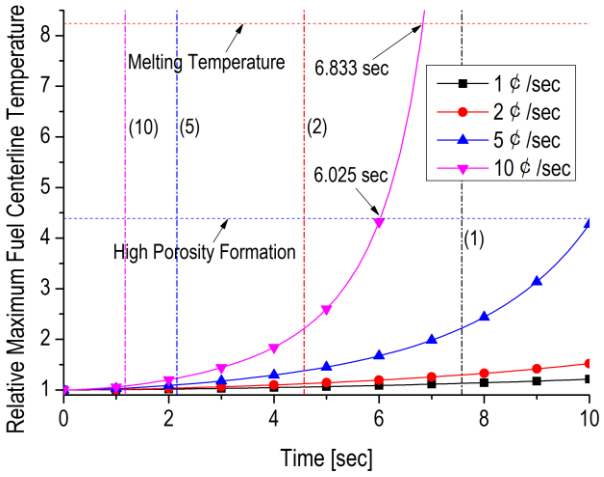


Fig. 2. Evolution of fuel temperature (constant mass flow rate).

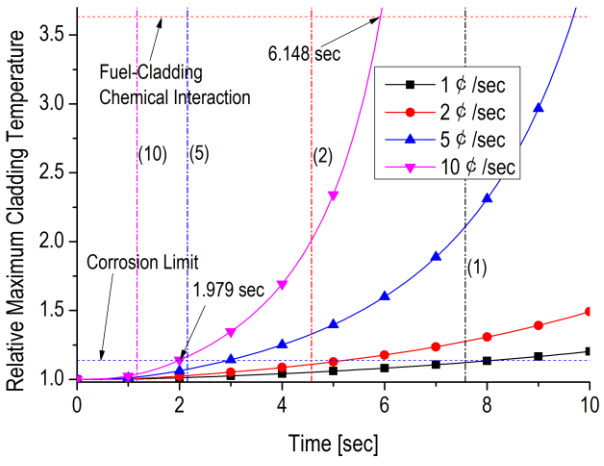


Fig. 3. Evolution of cladding temperature (constant mass flow rate).

Next, the coolant mass flow rate is simultaneously updated based upon the momentum integral equation. Figure 4 shows the development of the coolant mass flow rate (relative with respect to steady state value) as the thermal power is increased over time. As shown in Figure 5, the increased heat transfer from the fuel pin to

coolant slightly slowed down the increase of the temperature.

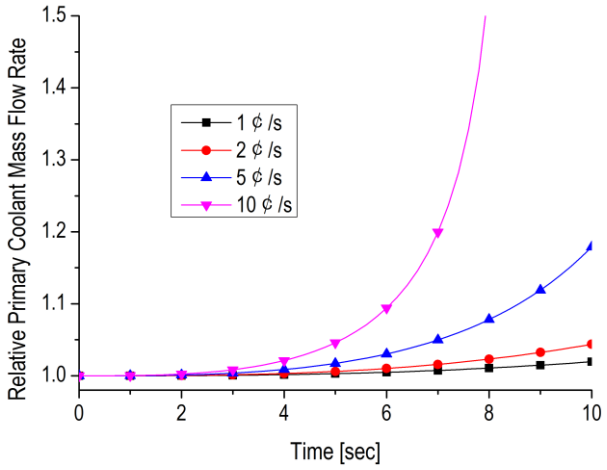


Fig. 4. Evolution of mass flow rate (variable mass flow rate).

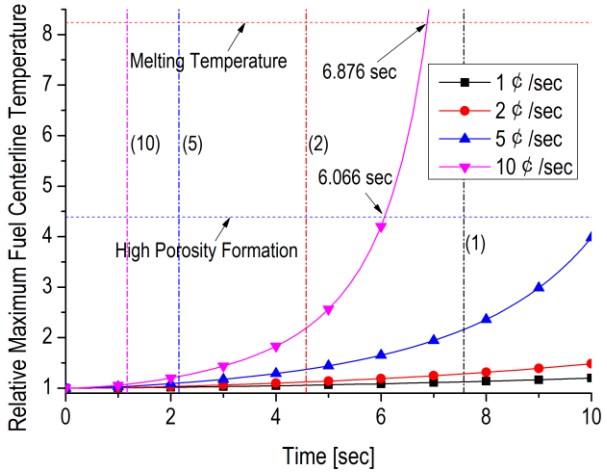


Fig. 5. Evolution of fuel temperature (variable mass flow rate).

Then, the temperature reactivity feedback is additionally considered. Figure 6 shows the change in heat generation rate (relative with respect to full power) along with reactivity components for the case of 1 cents/sec of ramp reactivity insertion. We can see that the increase of total reactivity is reduced by negative temperature feedback effect, leading to slower power increase. It is seen than the most of the decrease is due to the negative feedback from the coolant thermal expansion. In addition to this, it is observed from Figs. 7 and 8 that the inclusion of the reactivity feedback delayed the time when the fuel temperatures exceeds engineering constraints, giving more room for the safety actions. Also, from the above figure, it is seen that the higher peak cladding temperature is reached at the 115% power setpoint for smaller reactivity insertion. This is because the stored energy inside the fuel pin (shaded area in the figure), which is evaluated by subtracting power to coolant from the fission power and integrating it over time, is higher for the smaller ramp case, as depicted in Fig. 9 [8].

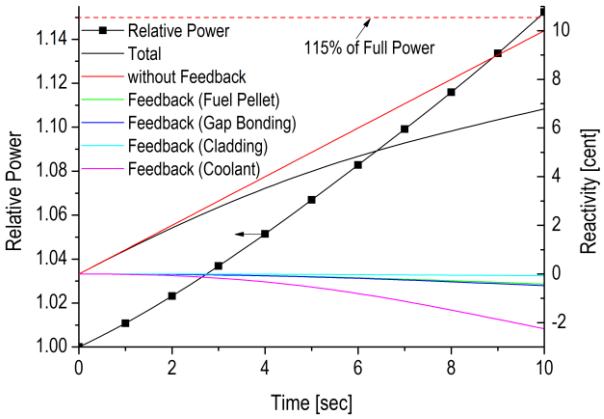


Fig. 6. Evolution of core power (with temperature feedback).

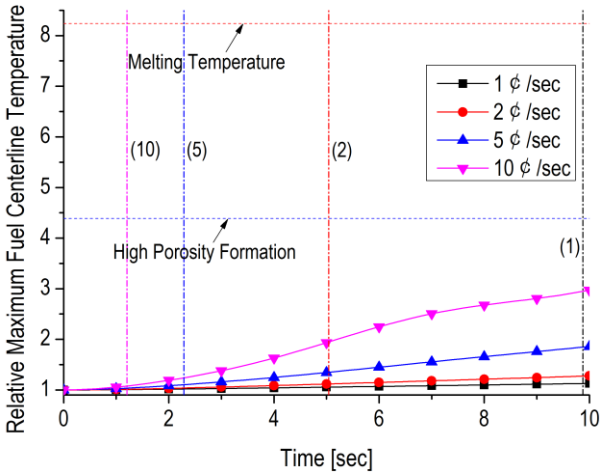


Fig. 7. Evolution of fuel temperature (with temperature feedback).

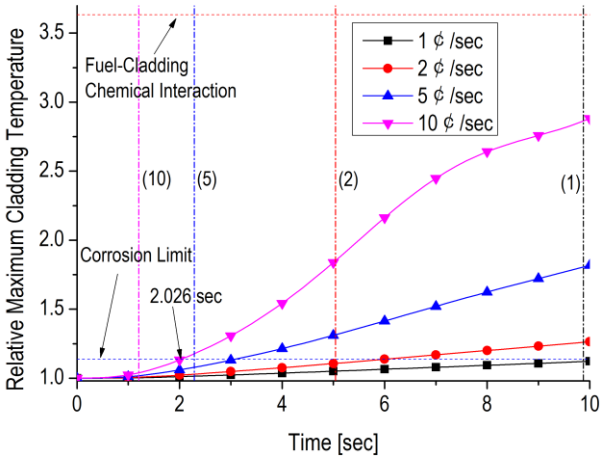


Fig. 8. Evolution of cladding temperature (with temperature feedback).

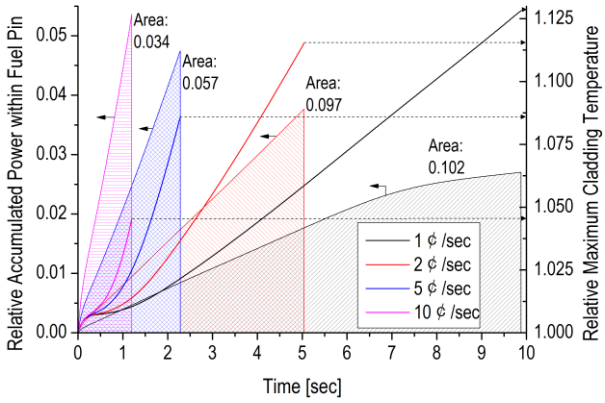


Fig. 9. Accumulated core power, energy and maximum cladding temperature rise.

## 3. Conclusions

Utilizing an in-house system analysis code, a set of numerical simulation is carried out on the reactivity ramp insertion transients which showed that the role of reactivity feedback is significant in mitigating the time to failure, and the evolution of the natural circulation mass flow is rather slow to generate meaningful feedback effect. It is also observed that in terms of the peak cladding temperature, smaller reactivity insertion transient generated more severe outcome owing to increased accumulation of the thermal energy within fuel pins. Thus, it may require an extra attention to carefully monitor and capture the mild transients to avoid potential drastic results.

## REFERENCES

[1] A. E. Walter et al., Fast Spectrum Reactors, Springer, NY, 2012.
[2] S. Glasstone, A. Sesonske, Nuclear Reactor Engineering, NY, 1967,
[3] H. J. Shim et al, McCARD: Monte Carlo Code for Advanced Reactor Design and Analysis, Nuclear Engineering and Technology, Vol. 44, p.161, 2012.
[4] J. E. Meyer, Hydrodynamic Models for the Treatment of Reactor Thermal Transients, Nuclear Science and Engineering, Vol. 10, p. 269, 1961.
[5] J. H. Ferziger, Numerical Methods for Engineering Application, John Wiley and Sons, NY, 1981.
[6] D. V. Hutton, Fundamentals of Finite Element Analysis, McGraw-Hill, NY, 2004.
[7] E. E. Lewis, Nuclear Power Reactor Safety, John Wiley & Sons, NY, 1977.
[8] Y. S. Tang et al., Thermal Analysis of Liquid-Metal Fast Breeder Reactors, American Nuclear Society, IL, 1978.